21st Australasian Fluid Mechanics Conference
Adelaide, Australia
10-13 December 2018

Examining flow dynamics of platelet function in micro-contractions using micro-PIV

F. Akbaridoust[1], C. M. de Silva[1], R. J. Brazilek[2], X. Chen[1], F. J. Tovar-Lopez[3] , E. Poon[1], A. Ooi[1], A. Mitchell[3], H. Nandurkar[2], W. S. Nesbitt[2,3] and I. Marusic[1]

[1]Department of Mechanical Engineering
University of Melbourne, Victoria 3010, Australia

[2]Australian Centre for Blood Diseases
Monash University, Victoria 3004, Australia

[3]School of Engineering
RMIT University, Victoria 3000, Australia

Abstract

This study examines the flow field in the near-vicinity of micro-contraction-expansion geometries in microfluidic devices designed to specifically examine the impact of flow acceleration on platelet function. To this end, a set of Micron-resolution Particle Image Velocimetry (micro-PIV) measurements is conducted under a specific set of shear flow gradient conditions with both Newtonian (water) and non-Newtonian (blood analog solutions) fluids. These experiments are complemented by numerical simulations and a set of measurements at matched conditions using blood platelets labelled with $DiOC_6$ (1μg/mL), introduced into the citrated human whole blood. Preliminary results reveal a good agreement between the experiments and numerical simulations at matched flow conditions. However, the experiments with blood analog solutions appear to exhibit different flow patterns both downstream and upstream of the micro-contractions. Furthermore, comparisons between the micro-PIV and blood flow experiments reveal that platelet aggregation appears to coincide with regions of high strain rate and wall shear stress. Collectively, these findings provide a better understanding of the appropriate simplifications that can be made in numerical and experimental work and provides a platform for future works to better understand the impact of flow acceleration on platelet activation.

Introduction

The blood flow in our body is complex and rich with fluid dynamics and is influenced by a number of factors which include: the vessel geometry, tissue properties associated with vessel compliance, and the physical properties of the blood. Of particular interest has been the examination of the flow dynamics that lead to platelet activation, which usually occurs where blood flow is disturbed for example after a vascular injury or stenosis. More specifically, blood-flow strain rate and its gradients play a critical role in initiating platelet activation at sites of arterial stenosis. Platelets can experience significant peak shear stresses/rates and elongation forces during flow accelerations at stenosis [9, 4]. A large body of work to date has focused on the key biological effects of elevated wall shear rates and stress under constant laminar flow regimes. However, the impact of shear flow stresses and its gradients on platelet function are less understood.

Early works, both numerical and experimental have highlighted the critical role played by the vessel geometry/stenosis on platelet activation and thrombus formation. More recently, (see [6]) it has been shown that the flow dynamics in the near-vicinity of a stenosis is an important factor in determining the rate of platelet activation, particularly in regions of flow decelerations at sites of stenosis and downstream of formed thrombi. Based on these observations, Tovar-Lopez et al [9] measured the platelet aggregation based on the local strain rate micro-gradients in different micro-contraction geometries, mimicking the strain rates conditions of blood vessel geometries with a stenosis.

Blood as a fluid has shear-thinning and viscoelastic non-Newtonian characteristics. Therefore, unless experiments are conducted with blood samples careful consideration has to be given to the chosen fluid properties, in particular when studying small diameter vessels such as capillaries and arterioles. Despite this, several works still opt to use Newtonian fluids for both numerical and experimental investigations [5]. To overcome these challenges, a few studies [8] have reported some success using blood analog solutions by matching the shear rheology to blood samples. However, they conclude that different blood analog solutions can exhibit markedly different flow patterns, particularly near abrupt changes in geometry such as a stenosis.

Accordingly, in the present study, we aim to provide a platform to study the impact of shear flow acceleration and extensional flow on blood platelet activation in a set of micro-contraction-expansion channel geometries. More specifically, we conduct a series of micro-PIV measurements, which are complemented by a set of experiments using whole blood at matched flow conditions. Preliminary comparisons are also drawn with numerical simulation results and blood analog solution experiments, providing us with a comprehensive set of data and tools to quantitatively examine the flow dynamics.

Experimental details

For the present study a set of microfluidic devices, each including four micro-contraction-expansion channels with different contraction angles of θ =7.5, 15, 40 and 80 degrees are fabricated using a soft-lithography technique (see figure 1). The micro-channels are fabricated with a width of 200 μm and a height of 100 μm and are composed of a micro-contraction ($\sim$stenosis) with a nominal width of 40 μm and maximum surface roughness of $\pm$300nm.

The microfluidic device is mounted onto the stage of a mo-

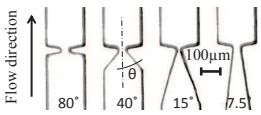

Figure 1: Micrograph of the fabricated micro-contraction-expansion geometries in a microfluidic device with different contraction angles of 7.5, 15, 40 and 80 degrees.

torised inverted Nikon Ti2 microscope containing a G-2A filter cube for epifluorescence imaging. For the first set of experiments, the four different micro-contraction geometries are tested primarily using distilled water (Newtonian fluid) at a flow rate of 45 μL/min using micro-PIV. The flow is seeded with one-micron diameter red fluorescent polystyrene aqueous spherical particles (ThermoFisher Scientific). A programmable syringe pump (Harvard PHD ULTRA) is used to withdraw the fluid from a reservoir through silicon tubes (0.020 in ID, 1/16in OD) to a 1000 μL gas-tight glass syringe (Hamilton).

The micro-PIV setup consists of a 15 Hz double-pulsed laser (70 mJ per 9 ns pulse, EverGreen - BigSky Laser Series) coupled with an external motorised attenuator module for illumination and a PCO.dimax HS4 camera (2000×2000 pixels, 12 bits) capable of capturing images at 2277 fps at full resolution. The microscope is equipped with a $40\times$ objective lens (CFI Super Plan Fluor ELWD, N.A.=0.6) providing an optical magnification of 0.27 μm/pixel and a depth of correlation of approximately 5.5 μm, which is estimated using the technique outlined in [7].

For the present experiments, micro-PIV measurements for all of the contractions are carried out in four different microfluidic chips to investigate the repeatability of experiments. In each set of measurements, 2000 pairs of images were recorded at 15 Hz. Each set of image pairs are processed using DAVIS (LaVision, GmbH) using standard PIV processing algorithms. More specifically, images are scaled based on a calibration grid and are then pre-processed using background image subtraction and by applying a histogram equalisation (see [2, 3, 1]). Further, to minimise interference from out-of-focus particles due to the reduced seeding density in micro-PIV measurements [10], two averaging methods, namely, 'Average Image Method' and 'Average Correlation Method' are employed to enhance the signal-to-noise ratio. Specifically, in Average Image Method, we overlay 20 images to increase the number of particles per interrogation window and the correlation between image pairs for the whole dataset ($\sim$1000 image pairs per dataset) are averaged.

Velocity vector evaluation is performed based on a cross-correlation algorithm using multi-grid with window deformation applied at each pass. Two multigrid passes are performed in all measurements, with the final window sizes of 32×32 pixels ($\sim$8.5 μm). A 75% overlap is employed for all images at the final interrogation window size, and any spurious vectors are identified using a median test [11] in a post-processing step.

Biological experiments

A set of experiments with blood are conducted at matched flow conditions (45 μL/min) to micro-PIV experiments to monitor platelet aggregation (see [6] for blood properties). For these experiments, the PDMS channels were allowed to passively adhere to ethanol/HCl-washed #1 borosilicate coverslips that formed the bottom channel wall and also acted as the imaging window. Ten minutes prior to blood sample loading, the microfluidic device is derivatized with purified human von Willebrand Factor (VWF) (100 $\mu g.ml^{-1}$) isolated from BioState® (CSL Ltd), according to previously published methods [4], to allow for effective platelet capture and adhesion to the PDMS surface. VWF is introduced via manual aspiration up to and including the micro-contraction apex and allowed to physisorb for 10 minutes at room temperature, before being aspirated via the same port. The chips are then subsequently perfused with bovine serum albumin (BSA- 10 $\mu g.ml^{-1}$) for a further 10 minutes in order to passivate all non-VWF-coated upstream segments and the underlying coverslip.

To assess platelet aggregation as a function of micro-contraction architecture human whole blood samples is incubated with the lipophilic membrane dye $DiOC_6$ (1 μg/mL) (Molecular Probes) and 0.02 U/mL apyrase (to eliminate released ADP during blood collection) for 10 minutes at 37°C and subsequently perfused through the device at constant flow rates of 45 μL/min. Blood perfusion and platelet aggregation dynamics are monitored on an inverted Nikon TiU microscope (Nikon Plan Fluor 20x/0.50 objective) using an Andor Zyla sCMOS camera at 1fps for 210 seconds.

Numerical simulations

To compliment the experimental databases, a set of computational fluid dynamics (CFD) simulations of water are performed in the four channels shown in figure 1. These simulations solve the incompressible Navier–Stokes equations using the finite volume methodology in OpenFOAM (OpenCFD, Ltd., ESI group, Bracknell, UK). Further, the convective and diffusive terms are approximated by the central differencing scheme, and the fully implicit backward scheme is used for the unsteady term. The Pressure Implicit with Splitting of Operator (PISO) method is employed to decouple the pressure term from momentum equation and a convergence criterion of 10^{-6} is used for both velocity and pressure. The velocity-inlet boundary condition is matched to the volumetric flow rate of the experiments (45 μL/min), and a zero gradient is applied at the inlet for pressure. At the outlet, a zero gradient is applied to the velocity coupled with a zero pressure.

Tetrahedral mesh elements are used for all four channel geometries and the meshes are completed in Pointwise (Pointwise, Inc., Fort Worth, Texas, USA), with a total mesh size ranging from 1.7 to 2.5 million elements. We note, the surface mesh resolution in the near vicinity of the constriction is refined to accurately capture any possible chaotic flow in this region. Further, in order to attain a fully developed statistically converged channel flow profile at the inlet similar to the experiments, a sufficiently long development section was included for the simulations. The development length for all cases was at least $20w$, where w is the width of the channel. The velocity profiles were verified at multiple locations prior to the contraction to ensure they are independent of the stream-wise location.

Results

To examine the differences in flow patterns at different contraction angles, θ, figure 2 presents the ensemble-averaged stream-wise velocity contours in the mid-plane (channel half-height) of the micro-contractions. Results are presented for the experiments at $\theta = 40^\circ$ and $\theta = 7.5^\circ$ using water at a flow rate of

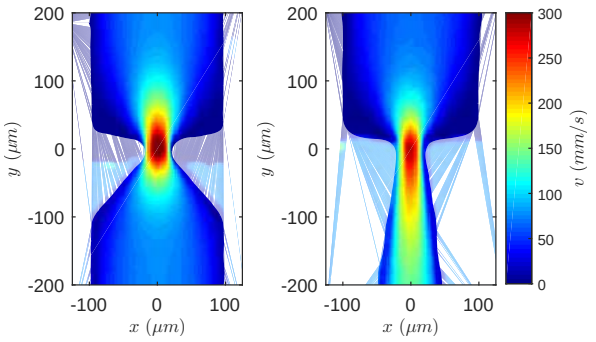

Figure 2: The ensemble-averaged stream-wise velocity contours at the mid-plane of micro-channels with a contraction angle of 40° (left) and 7.5° (right). Results are presented at a flow rate of 45 μL/min.

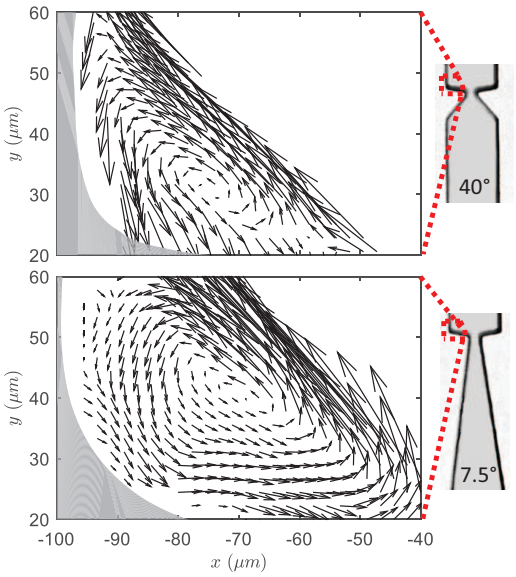

Figure 3: Magnified view of the velocity vector field of the expansion corners for the two micro-contraction configuration shown in figure 2. (top) $\theta = 40^{\circ}$ and (bottom) $\theta = 7.5^{\circ}$.

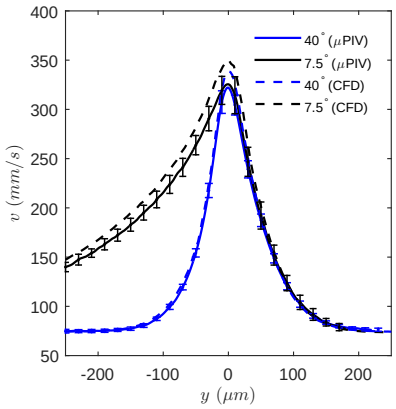

Figure 4: Profiles of stream-wise velocity at the centreline of the channel from the micro-PIV (solid lines) and numerical simulations (dashed lines). Results are presented for contraction angles of $\theta = 40^{\circ}$ and $\theta = 7.5^{\circ}$ at the flow rate of 45 μL/min. The error bars ($\pm$ standard deviation) show the repeatability of experiments and is computed from four independent experiments for each case at matched conditions.

45 μL/min. Qualitatively, the high-speed region is more pronounced prior to the contraction at smaller θ due to the narrower inlet geometry. In contrast, immediately after the contraction the downstream flow patterns only have a subtle difference between the two cases compared, due to the similar channel geometry after the contraction. However, upon closer inspection, we observe two recirculation regions in the expansion corner after the micro-contraction at both $\theta = 7.5^{\circ}$ and $\theta = 40^{\circ}$ (c.f. figure 3). Upon closer inspection, at smaller θ (figure 3 bottom) the results appear to exhibit larger/stronger recirculation zones, which might be a consequence of the slightly higher velocity on the centre plane at the contraction, which in turn leads to stronger decelerations immediately after the contraction (c.f. figure 4).

To quantify the velocity profile at different contraction angles, θ, figure 4 shows the stream-wise velocity profile at the centreline of the micro-channels. The solid and dashed lines correspond to results from the micro-PIV experiments and the numerical simulations, respectively, which appear to be in good agreement with a maximum discrepancy of 5% at the velocity peak. We note the error bars on the solid lines corresponds to the repeatability of experiments for the measurements carried out in different microfluidic chips, which shows a maximum deviation of 4.5%. This discrepancy is primarily due to the subtle difference in the channel height (maximum 2.5%), which is primarily caused by the accuracy in precisely locating the channel half height. Future experiments are planned to minimise these discrepancies across a wider range of contraction angles.

In order to visualise blood platelet activation at the micro-contractions, figures 5(a-c) present snapshots from epifluorescence imaging. The results are presented for the case $\theta = 80^{\circ}$ on a wall-parallel slice at the channel centreline in *z*-direction. The colour contours reveal that a strong region of platelet aggregation is present on the side-walls immediately after the contraction. To visualise the underlying flow patterns and acceleration figure 5(d) presents the strain rate (dv/dy) at matched flow conditions from the micro-PIV experiments. The results show that initial platelet recruitment (aggregate formation) appears to occur in regions where the flow strain is high at the wall at the apex of step geometry. Moreover, through the numerical simulation results, we observe that the shear stress (see figure 5e) is also at its highest on the side walls in this region.

Blood analog solution experiments

The results presented in the preceding discussions from the micro-PIV experiments are from a set of experiments using a Newtonian fluid (water). However, blood as a fluid exhibits shear-thinning and viscoelastic non-Newtonian characteristics, therefore in this section, we present preliminary findings from a set of micro-PIV experiments using a non-Newtonian solution. For the present case, we have chosen to use a solution of Xanthan gum (500 ppm w/w) based on works by [8]. However, as pointed out in their study, although the fluid exhibits shear thinning behaviour the fluid still differs from whole blood and results should be interpreted with caution. Further, due to limitations of the experimental setup, a lower flow rate of 4.5 μL/min is employed and results are only shown for a micro-contraction with an angle of $\theta = 40^{\circ}$.

Figure 6 shows the ensemble-averaged stream-wise velocity contours in the mid-plane (channel half-height) of the micro-contractions at matched conditions with water and the blood analog solution. The results show clear evidence of different flow patterns arising from the two fluids examined, albeit at a low flow rate. More specifically, the Xanthan gum solution appears to exhibit large recirculation zones prior to the micro-contraction (see figure 7), which is absent from the experiments using water at matched conditions. These results highlight the significance of employing fluids that have closer properties to whole blood, in future works.

Conclusions

This study employs micro-PIV measurements and numerical simulations to examine the effect of flow acceleration and deceleration at a stenosis on platelet function in a set of micro contraction-expansion channels. The micro-channels tested are constructed with a width of 200 μm and a height of 100 μm with a symmetric micro-contraction of 40 μm with different contraction inlet angles that applies an extensional flow at the stenosis entry. To complement these measurements an independent set of biological experiments are conducted using blood platelets labelled with $DiOC_6$ introduced into citrated human whole blood. Our results reveal good agreement between the

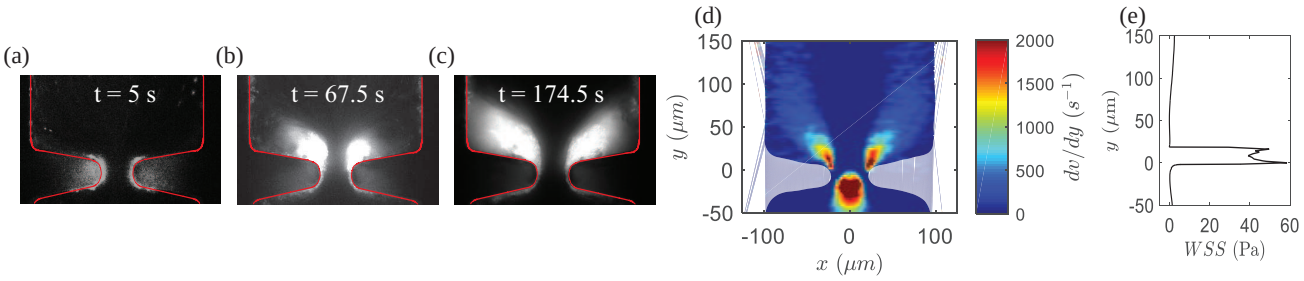

Figure 5: Snapshots from confocal imaging experiment, where colour contours correspond to blood platelets which have been labelled with $DiOC_6$ (1μg/mL). (a) $t = 5$ s, (b) $t = 67.5$ s and (c) $t = 174.5$ s. (d) Flow strain rate (dv/dy) at the mid-plane from micro-PIV experiments and (e) shows the wall shear stress from the numerical simulations. All results are presented for a contraction angle of 80° at a flow rate of 45 μL/min.

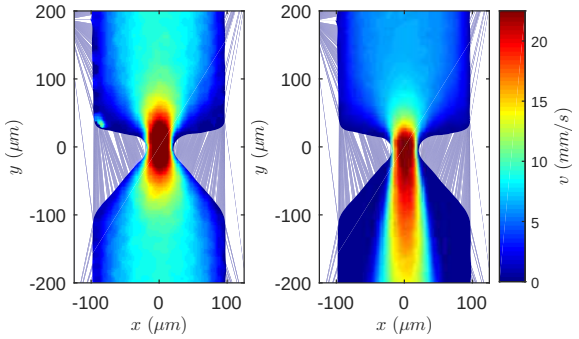

Figure 6: The ensemble-averaged stream-wise velocity contours at the mid-plane of micro-channels with a contraction angle of 40° for water (left) and xanthan gum solution (right). Results are presented at a flow rate of 4.5 μL/min.

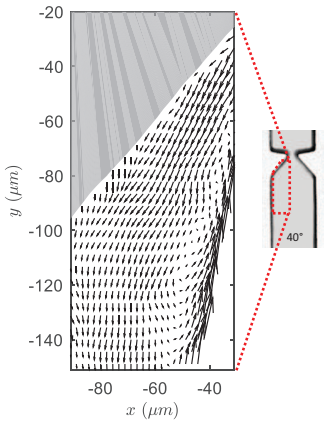

Figure 7: Xanthan gum flow recirculation in the contraction corner of micro-channel with the contraction angle degree of 40° at the flow rate of 4.5 μL/min.

micro-PIV and numerical simulations at matched flow conditions. Further, a comparison to the biological experiments appear to provide support that the initiation of platelet aggregation coincides with high strain rate zones near the wall that also coincide with increased wall shear stress. Collectively, these findings can be used to improve numerical models and also provide a platform for future works to better understand the impact of flow acceleration at stenosis on platelet activation.

Acknowledgements

The authors wish to gratefully thank the financial support of the Australian Research Council.

References

[1] Akbaridoust, F., *Characterisation of a microfluidic hydrotrap to study the effect of straining flow on waterborne microorganisms*, Ph.D. thesis, University of Melbourne, 2017.

[2] Akbaridoust, F., Philip, J. and Marusic, I., A miniature high strain rate device, *Proc. 20th AFMC. Conf.*.

[3] Akbaridoust, F., Philip, J. and Marusic, I., Assessment of a miniature four-roll mill and a cross-slot microchannel for high-strain-rate stagnation point flows, *Meas. Sci. Tech.*, **29**, 2018, 045302.

[4] Brazilek, R. J., Tovar-Lopez, F. J., Wong, A. K., Tran, H., Davis, A. S., McFadyen, J. D., Kaplan, Z., Chunilal, S., Jackson, S. P., Nandurkar, H. et al., Application of a strain rate gradient microfluidic device to von willebrand's disease screening, *Lab Chip*, **17**, 2017, 2595–2608.

[5] Cherry, E. M. and Eaton, J. K., Shear thinning effects on blood flow in straight and curved tubes, *Phys. Fluids*, **25**, 2013, 073104.

[6] Nesbitt, W. S., Westein, E., Tovar-Lopez, F. J., Tolouei, E., Mitchell, A., Fu, J., Carberry, J., Fouras, A. and Jackson, S. P., A shear gradient–dependent platelet aggregation mechanism drives thrombus formation, *Nat. Med.*, **15**, 2009, 665.

[7] Olsen, M. G. and Adrian, R. J., Out-of-focus effects on particle image visibility and correlation in microscopic particle image velocimetry, *Exp. Fluids*, **29**, 2000, S166–S174.

[8] Sousa, P., Pinho, F., Oliveira, M. and Alves, M., Extensional flow of blood analog solutions in microfluidic devices, *Biomicrofluidics*, **5**, 2011, 014108.

[9] Tovar-Lopez, F. J., Rosengarten, G., Westein, E., Khoshmanesh, K., Jackson, S. P., Mitchell, A. and Nesbitt, W. S., A microfluidics device to monitor platelet aggregation dynamics in response to strain rate micro-gradients in flowing blood, *Lab Chip*, **10**, 2010, 291–302.

[10] Wereley, S. T., Gui, L. and Meinhart, C. D., Advanced algorithms for microscale particle image velocimetry, *AIAA*, **40**, 2002, 1047–1055.

[11] Westerweel, J. and Scarano, F., Universal outlier detection for PIV data, *Exp. Fluids*, **39**, 2005, 1096–1100.